Strength and damage of concrete under high triaxial loading

Yann Malecot - Laurent Daudeville - Fabrice Dupray – Cédric Poinard – Eric Buzaud

Université Joseph Fourier – Grenoble I
Laboratoire Sols, Solides, Structures - Risques, CNRS
BP53, 38041 Grenoble Cedex 9
France
yann.malecot@ujf-grenoble.fr

ABSTRACT. This study focuses on identifying concrete behavior under severe loading (near field detonation or ballistic impacts). In order to reproduce high stress levels with well-controlled loading paths, static tests are carried out on concrete samples by mean of a very high-capacity triaxial press. Experimental results indicate a sizable change in concrete behavior with confining pressure. At low pressure values, the concrete exhibits brittle behavior with failure caused by a localized damage mechanism. In contrast, at high confining pressures, the concrete becomes a ductile material, and failure is associated with diffuse material damage. These tests also show an evolution of the elastic characteristics of concrete. A numerical modeling of these previous experiments is performed at a mesoscopic scale. It provides a reproduction of the main characteristics of concrete behavior under high confinement, both qualitatively and quantitatively.

RÉSUMÉ. Cette étude vise à caractériser le comportement du béton sous chargement sévère (explosion en champ proche ou impact balistique). Afin de reproduire de forts niveaux de contrainte avec un chemin de chargement bien contrôlé, des tests statiques sont réalisés à l'aide d'une presse de grande capacité. Les résultats montrent une importante modification du comportement du béton avec le confinement. A faible confinement, le béton a un comportement fragile avec une rupture provoquée par un mécanisme d'endommagement localisé. A l'inverse, à fort confinement, le béton est ductile et la rupture est associée à un endommagement diffus du matériau. Ces essais montrent également une évolution des caractéristiques élastiques du béton. Une modélisation numérique des expériences précédentes est ensuite réalisée à l'échelle mésoscopique. Elle permet de reproduire, à la fois qualitativement et quantitativement les principales caractéristiques du comportement du béton sous fort confinement.

KEY WORDS: concrete, triaxial test, high confinement, mesoscale modeling, Young's modulus.

MOTS-CLÉS: béton, essai triaxial, fort confinement, modèle mésoscopique, module d'Young.

1. Introduction

Concrete is the most widely used manufactured material in the world. In particular, it is employed in the building of highly-sensitive infrastructures (civil engineering structures, dams, nuclear power plants, etc.). Its mechanical behavior however is still rather poorly understood, especially under extreme loadings. This article focuses on the behavior of concrete under near-field detonations or ballistic impacts. During such loadings, concrete undergoes very high-intensity stress states (Zukas 92). In exceptional cases, an impact may cause complete perforation of the target. The validation of constitutive models, which take the phenomena of brittle damage and irreversible strain into account, thus requires experimental procedures capable of reproducing complex loading paths.

Most experimental results available in the literature only address triaxial loadings with a moderate level of confining pressure (Li *et al.* 1970, Kupfer *et al.* 1973, Wang *et al.* 1987, Jiang *et al.* 1991, Imran *et al.* 1996, Taliercio *et al.* 1999, Sfer *et al.* 2002). In particular, these authors have revealed the transition from brittle to ductile behavior in characterizing cohesive materials. The results presented in this article refer to triaxial compression tests conducted on concrete samples by means of a high-capacity hydraulic triaxial press, called GIGA. This experimental device makes it possible to generate stress levels within the samples on the order of 1 GPa with static, homogeneous and well-controlled loading paths.

Deriving the static characterization of a constitutive model for the purpose of predicting dynamic calculations is not a new practice within the study of geomaterials. Indeed, dynamic strain compression tests showed that the deviatoric and hydrostatic behaviors of mortars appear almost independent of the strain (Forquin *et al.* 2008). Previous static experimental studies have essentially been limited to mortar samples (Bazant *et al.* 1986, Burlion *et al.* 2001, William EM *et al.* 2005); such studies emphasize both the increase in mortar deviatoric stress and the evolution in mortar limit states with confinement. The aim of the present paper is to extend this practice to the study of an "actual" concrete material (i.e. with an aggregate dimension on the order of a centimeter). The comparative evaluation between a concrete and a mortar with confining pressure reaching 500 MPa (Akers *et al.* 2004), highlights the differences in behavior between two materials and moreover reveals that the study of mortar with strong confinement is not representative of concrete behavior. Other triaxial test results on ordinary concrete with confining pressures ranging between 0 and 500 MPa yield the evolution in concrete behavior and limit states with confinement (Warren *et al.* 2004, Schmidt *et al.* 2008, Gabet *et al.* 2008).

In 2004, the university of Grenoble launched, in collaboration with the Centre d'Etude de Gramat (DGA, French Defense Ministry), a research program on the vulnerability of concrete infrastructure. This study has demonstrated the possibility of performing, in a reliable manner, triaxial compression and extension tests at high confinement pressures on porous concrete specimens with a controlled degree of

saturation (Hong *et al.* 2009a). Thanks to the innovative experimental device developed during this study, the initial experimental campaigns focused on the influence of loading path (Gabet *et al.* 2008, Poinard *et al.* 2009), water/cement ratio (Hong *et al.* 2009b) and saturation degree (Hong *et al.* 2009c) on the concrete behavior under high confinement. This device also allowed studying the mortar behavior under high stress level (Dupray *et al.* 2009).

The study presented herein is aimed at completing these previous research efforts by focusing on the concrete strength and failure mechanism for triaxial compression tests ranging from simple compression to 650 MPa of confinement. The experimental devices is described in Section 2. Test results which show the effects of an increase in confinement on concrete behavior, in particular on damage evolution, is presented next in Section 3. A damage-plasticity model is then used to model the behavior of mortar and to create a mesoscopic model of the concrete sample. A comparison between numerical and experimental tests is presented for hydrostatic and triaxial compression in Section 4. The article is closed in Section 5 with a discussion of the results of this study.

2. Experimental device

2.1. *Triaxial cell*

The tests have been conducted with a high-capacity triaxial press that allows loading a cylindrical concrete specimen 7 cm in diameter and 14 cm long. Figure 1 (left) shows a general view of the press. A cross-section of the confining cell is provided in Figure 1 (right). This press is able to generate a confining pressure of up to 0.85 GPa and an axial stress reaching 2.3 GPa. The concrete specimen is placed in the confining cell, and the confining fluid, diethylhexyl azelate - a non-volatile organic liquid, is injected into the cell through the upper opening. The cell is then pressurized by means of a multiplying jack. The axial force is generated from a 13-MN jack placed underneath the cell; this force is transmitted to the specimen via a piston that passes through the lower cell plug. An axial displacement sensor located on the machine is used to control axial jack displacement, while an axial load sensor and pressure sensor positioned inside the confining cell yield the stress state on the specimen. Both the confining pressure and jack axial displacement are servo-controlled, which offers several potential loading paths.

2.2. *Preparation of concrete samples*

The concrete composition is provided in Table 1. This mix proportioning corresponds to an ordinary concrete in terms of both strength and slump. After pouring, the concrete blocks were conserved for one month in water and then

machined and stocked for two months in a drying oven at 50°C, which made the concrete practically dry at the time of testing (i.e. with a saturation level of concrete equal to approximately 11%). The level of strain is measured by means of an axial LVDT sensor, an axial gauge and two circumferential gauges. Strain measurement redundancy serves to check sample strain homogeneity. Considering the porous nature of concrete, this high level of confining pressure has necessitated developing a protective multilayer membrane wrapped around the sample, composed of 8 mm of latex and 2 mm of neoprene (Gabet *et al.* 2006, Hong *et al.* 2009a).

2.3. *Loading path*

Except for the unconfined compression tests, all triaxial compression tests have been carried out using a similar loading path of the triaxial compression type. The test begins with a hydrostatic phase, during which confining pressure increases at a rate of 1.67 MPa/sec until reaching the desired confining pressure. The deviatoric phase is then conducted, at constant confining pressure, by imposing a constant displacement rate of 20µm/sec for the axial jack. This rate corresponds to a strain rate of approximately 10^{-4}/sec for the sample. Note that the maximum deviatoric stress value is not imposed but is a result of the test. It should be noted that stresses are counted as positive in compression. σ_x denotes axial stress, p the confining pressure, σ_m the mean stress, and q the scalar deviatoric stress, i.e.

$$\sigma_m = \frac{\sigma_x + 2p}{3} \qquad [1]$$

$$q = \sigma_x - p \qquad [2]$$

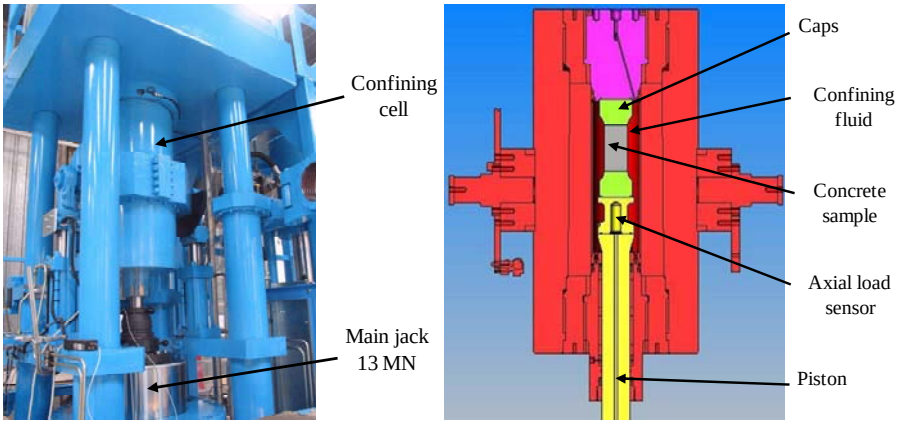

Figure 1. General view of the GIGA press (left); Cross-section of the confining cell (right)

Table 1. Compositions and mechanical properties of the studied concrete.

Concrete composition	
0.5/8 "D" gravel (kg/m^3)	1,008
1,800 µm "D" sand (kg/m^3)	838
CEM I 52.5 N PM ES CP2 cement (Vicat) (kg/m^3)	263
Water (kg/m^3)	169
Density (kg/m^3)	2,278
Mechanical properties of the concretes	
Average tested strength after 28 days (MPa)	29
Average slump measured using the Abrams cone (cm)	7
Volume of entrained air in fresh concrete (%)	3.4
Porosity accessible to water (%)	12
W/C ratio	0.64
Cement paste volume V_p (m^3/m^3)	0.252

2.4. *Optical observations*

To complete this experimental study, optical observations were recorded in order to characterize concrete damage in the sample. These observations took place at the mesoscopic scale (characteristic aggregate size) by use of simple binocular. All samples observed were first tested until failure, except for the one corresponding to the hydrostatic test.

Meticulous preparation is required prior to undertaking an optical analysis of the post-test sample. During the initial step, the sample is immersed in epoxy resin. This step takes place in a vacuum cell and is intended to freeze the residual damage of the broken sample. The sample is then diametrically cut with a diamond wire saw. Once the sample has been split into two parts, the desired sample surface is impregnated with resin. The final step consists of polishing this surface.

3. Test results

Axial strain is obtained from the axial gauge at the beginning of the test. Should the gauge fail or the measurement become meaningless, the LVDT sensor is employed for the end of the test. Circumferential strain is derived by taking the mean of the two circumferential gauge readings, whereas volumetric strain is deduced from these same two measurements in assuming that the concrete radial strain is similar to the circumferential strain, i.e.:

$$\varepsilon_v = \varepsilon_x + 2\varepsilon_\theta \qquad [3]$$

3.1. *Hydrostatic test*

Figure 2 (left) shows a volumetric behavior curve corresponding to a hydrostatic load with unloading-reloading cycles. The upper envelope indicates a major modification in the tangent bulk modulus of concrete. For a mean stress of less than 60 MPa, this modulus does not evolve significantly. The concrete behavior is said to be linear elastic. The first five unloading-reloading cycles are thus similar. From 60 MPa on up, the tangent modulus decreases substantially, with this drop most likely being due to cement matrix damage. At a mean stress of about 250 MPa, an inflection point is observed, after which concrete stiffness resumes. This stiffening phase corresponds to an increase in material contact caused by the abrupt decline in porosity (Balmer 49).

The unloading cycles occurring during the test allow evaluating both the irreversible strain and the evolution in residual bulk elastic modulus. The first irreversible strains begin to appear after the decrease in tangent modulus. A permanent volumetric strain of 0.02% is measured after one cycle at 80 MPa of confining pressure. For the last unloading cycle, an inelastic strain of about 4% is obtained for a load at 580 MPa. Note the very strong nonlinearity at the completion of unloading, which returns the residual volumetric strain of concrete to less than 2%. This sudden decrease in tangent modulus is probably due to cement matrix damage when the granular skeleton, which remains elastic, recovers its initial shape.

Figure 2 (right) presents the bulk elastic modulus Kv corresponding to the linear part of the unloading cycle vs. confining pressure. Kv value increases monotonically with pressure. This increase proves to be significant for confining pressures below 150 MPa, at which point the cement matrix becomes heavily damaged. Afterwards, Kv increases from 14 GPa for pure concrete to 23 GPa for a 150 MPa confinement. The increase in Kv beyond 150 MPa however is very limited, since the Kv value only equals 24 GPa at 580 MPa. The volumetric behavior of concrete thus shows similarity with that of a high-friction granular material.

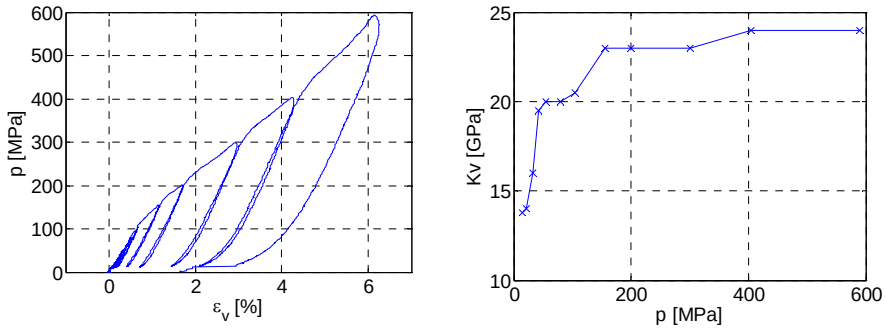

Figure 2. Hydrostatic (HYD) test: Confining pressure p vs. volumetric strain ε_v (left); Bulk elastic modulus in unloading vs. confining pressure p (right).

Figure 3 displays a comparison of concrete optical observations, between an undamaged sample, and a sample recovered after a 400 MPa hydrostatic loading (HYD400). A comparison of the two photographs shows a granular rearrangement associated with concrete compaction. This Figure clearly reveals a closure of macroscopic porosity along with damage at the cement matrix/aggregate interface, also called the interfacial transition zone (ITZ) or "transition aureole"; this interface is a zone of weakness within the cement matrix (Diamond *et al.* 2001) and can be seen on the photographs as a thin white band around the aggregates. On the sample tested along a hydrostatic loading path, the ITZ is much more distinct than on the undamaged sample, which thus reflects a localization of concrete damage on this interface that can be explained by both the weakness in this zone and the discontinuity in mechanical properties between aggregates and matrix.

Other phenomena demonstrate that the concrete has lost a sizable amount of its cohesion. When observing the surface of the sample without resin after cutting, a number of small zones are visible where the mortar disintegrates very easily (see Figure 4). This loss of cohesion in the cement matrix is caused by the hydrostatic load and then amplified when the sample is cut. These optical observations also reveal the presence of some unbounded or stamped aggregates.

This hydrostatic test and associated optical observations provide a better understanding of the hydrostatic behavior of concrete. At low confining pressures (less than 150 MPa), behavior is governed by the porous and cohesive cement matrix, which leads to a strong decrease in the volumetric tangent stiffness of concrete at the onset of the compaction process. For intermediate confining pressures (from 150 to 400 MPa), the cement matrix loses a portion of its cohesion, in which case the concrete behaves like a compact granular stacking arrangement, i.e. elastoplastic behavior with a constant elastic unloading modulus. For the highest confining pressure level (beyond 400 MPa), the drop in porosity and concrete densification are both significant and constitute a rise in volumetric tangent stiffness.

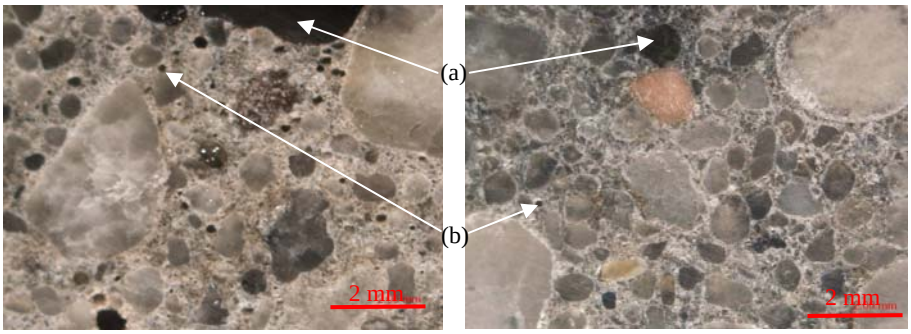

Figure 3. Photograph of the center of the sample: reference specimens (left) and HYD400 test specimens (right); (a) large pores filled with resin; (b) small pores without resin.

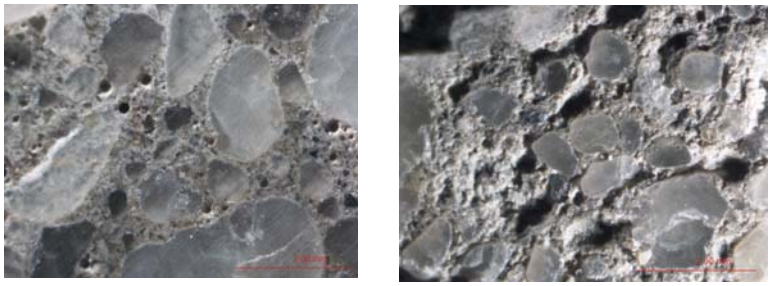

Figure 4. Photograph of concrete at the center of the sample: reference specimens (left) and HYD400 specimens in a zone where the mortar is crumbling (right).

The unloading behavior, which started out linear, is no longer linear at the end of unloading, with a concrete stiffness value that decreases very sharply. This phenomenon is due to the heterogeneous nature of concrete. The granular skeleton, which remains basically elastic, recovers its initial shape and causes damage to the cement matrix, which had been strongly compacted during hydrostatic compression.

3.2. *Triaxial tests*

It is a well-known fact that geomaterials are pressure-dependent; triaxial test results are therefore typically analyzed in the (J, σ_m) plane, where σ_m is the mean stress and J the Von-Mises stress ($J = \sqrt{3J2}$, with J2 being the second deviatoric stress invariant). In the present study, $J = \|q\|$, where q = σ_x - p is the principal differential stress.

3.2.1. *Unconfined compression test*

The unconfined compression test consists of a triaxial test undertaken at a zero confining pressure. Figure 5a displays a set of curves of axial stress vs. strain components. For axial stress values below 20 MPa, the unloading-reloading cycles overlap, the concrete behaves in an elastic linear manner. Young's modulus equals 33 GPa and Poisson's ratio stands at 0.16. Beyond 20 MPa of axial stress, the tangent modulus decreases continuously until reaching a peak stress at around 40 MPa. The concrete then has a softening behavior. In investigating the unloading-reloading cycles, a continuous decrease in unloading modulus is apparent during the test once the elastic phase has been completed, with a drop from 35 GPa for the first cycles to 7 GPa by the end of the test. The slight increase in stiffness, found at the beginning of compression, can be explained by the closure of the initial cracks created during drying. The subsequent decrease is caused by the gradual damage of concrete during compression. The hysteresis loops observed after the peak stress are characteristic of localized damage, which is consistent with sample observations

during the test and information available from the literature (Sfer *et al.* 2002, Torrenti *et al.* 1993). These findings reveal axial cracking of the sample during compression, in which case concrete behavior is characteristic of a brittle material governed by damage phenomena.

3.2.2. *Triaxial tests at 20 MPa and 50 MPa*

The triaxial test results at 20 MPa and 50 MPa yield similar results, the comments offered on the curves are then based primarily on the test conducted at 20MPa of confinement, whose noise level is slightly lower. The deviatoric part of tests depicted on the curves in Figures 5b displays similar characteristics to those observed during the unconfined compression test. Following an elastic phase, the tangent modulus decreases and concrete behavior then becomes dilating. Next, a peak stress is reached before the concrete softens.

In spite of these similarities, these Figures still show the effect of confinement on concrete behavior. A very sharp rise in strength is noticed with the maximum deviatoric stress increasing from 40 MPa for the simple compression test to 135 MPa for the TRX20 test. Moreover, the concrete becomes more ductile as the TRX20 test displays a stress plateau, with an axial strain measured of about 4%.

The first unloading-reloading cycles are linear elastic. Like with the simple compression test, the material hardens slightly, followed by a modulus decrease with an increase in axial strain. This decrease, synonymous with damage, is smaller than that recorded during the simple compression test. Note that the hysteresis phenomenon observed during unloading-reloading cycles is clearly less discernible as confinement increases.

Figure 6 contains a photograph of the cylindrical face of the TRX50 sample after the triaxial test at a confinement of 50 MPa. The sample essentially shows localized damage, with failure being caused by the formation of just one or two thin cracks developing inside the material. The optical observation of the sample section cut reveals almost no damage in the matrix.

3.2.3. *Triaxial tests at 200 MPa and 400 MPa*

Figures 5c and 5d display triaxial test results for confining pressures of 200 MPa and 400 MPa, respectively. For a confinement of 400 MPa, the experimental device is not able to reach the peak stress; concrete behavior becomes ductile with a very high level of strain hardening. The volumetric curves beyond a certain threshold indicate however that concrete behavior changes from a contraction phase to a dilatancy phase (some volumetric curves are presented Figure 14a, section 4). This point of contraction-dilatancy transition allows defining a strain limit state for the concrete.

The unloading-reloading cycles on these tests show that Young's modulus evolves similarly as in previous tests. The variance in this modulus with respect to axial strain however is less pronounced as confining pressure increases. For the TRX400 test, Young's modulus only decreases therefore by a small amount, from 65 GPa at the beginning of axial loading to 58 GPa for an axial strain of about 6%. In addition, the hysteresis phenomenon between unloading and reloading becomes practically nonexistent for such a confinement level.

The concrete makes the transition from a very brittle behavior in the simple compression test to a ductile behavior with strain hardening subjected to a very high confinement. The study performed by Sfer indicates a similar trend but for substantially lower confining pressures (Sfer *et al.* 2002).

In order to better understand the failure mode of concrete under high confinement, Figure 7 display the optical observations recorded on the sample after a triaxial test at a confining pressure of 650 MPa and until reaching an axial strain of 12%. Figure 7 (left) shows a photograph of the full sample section cut. A thick crack, perpendicular to the compression test axis, crosses the sample by circumventing the aggregates. Other thinner cracks featuring the same orientation are also visible on the close-up of this section cut (middle and right of Fig. 7).

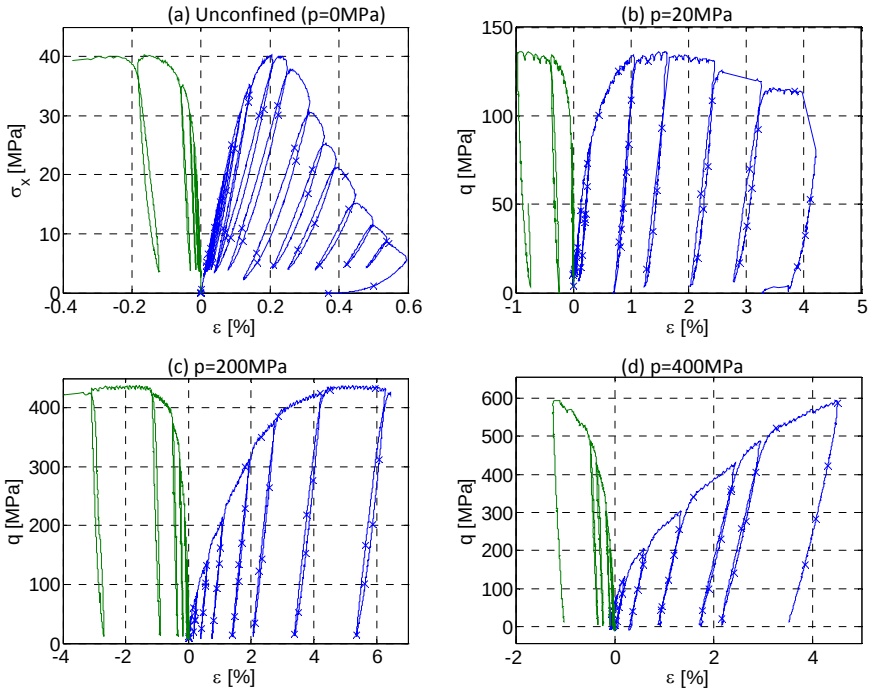

Figure 5. Triaxial tests: Axial stress σ_x vs. deviatoric strain components ε_x (×) and ε_θ (-); (a) Unconfined compression, (b) p=20MPa, (c) p=200MPa, (d) p=400MPa.

Figure 7 (middle) shows a very high level of damage for the cement matrix of concrete. This matrix has lost its cohesion and the visible porosity has completely disappeared. Around the larger aggregates, an interstice reveals the presence of considerable unbounding. Figure 7 (right) indicates an enlarging facies of the same sample in a zone without any coarse gravel. Many small cracks are visible in the matrix, and this characterizes diffuse damage. The orientation of these cracks is mainly perpendicular to the axial compression direction.

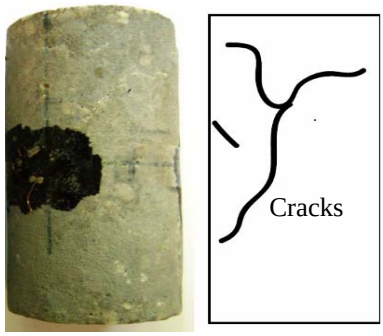

Figure 6. TRX50 specimen after a triaxial test at 50MPa confinement (left); condition of concrete on the cylinder-shaped surface (right).

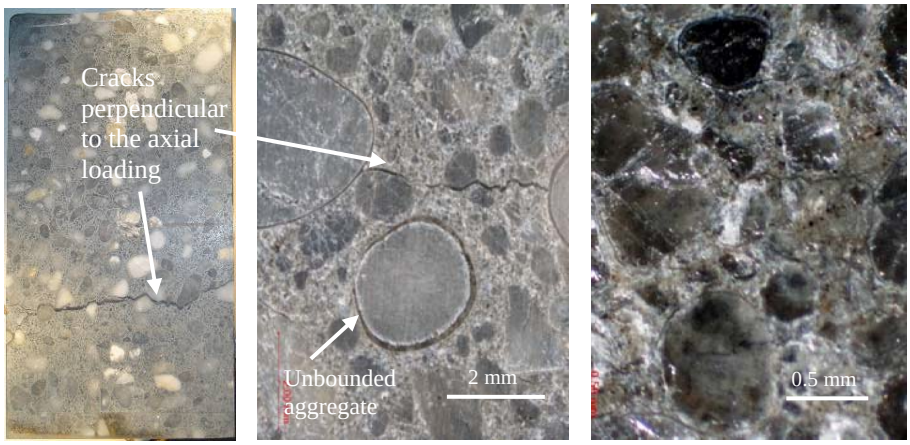

Figure 7. TRX650 half-sample after test (left); close-up (middle); cement paste damage on the TRX650 specimen.

3.3. *Evolution in concrete behavior with confinement*

3.3.1. *Evolution in elastic features*

The test results presented above show a major change in concrete behavior with confinement. In order to better quantify this evolution, this section of the paper provides a summary of the progression in concrete elastic features over the course of the previous tests. Figure 8 shows, for each test, the evolution in Young's modulus E_d and Poisson's ratio ν_d vs. axial strain ε_x. These parameters are identified by the average unloading-reloading cycle lines. The associated axial strain corresponds to the value obtained before initiating the unloading cycle.

Figure 8a indicates that the Young's modulus of concrete increases monotonically with respect to confining pressure and decreases with an increase in axial strain. This figure also clearly highlights that the decrease in E_d with axial strain becomes less pronounced as confinement increases. The concrete damage, as characterized by the decrease in E_d with strain, is therefore inhibited by confinement.

The evolution in ν_d is similar with an opposite sign. Figure 8b shows that Poisson's ratio increases considerably during the simple axial compression test. This well-known phenomenon can be explained by the opening of axial cracks during the simple compression test, which causes the dilating behavior of concrete. On the other hand, for higher confinement levels, Poisson's ratio increases only marginally during the test, which suggests that high confinement prevents cracks from opening during the compression phase.

3.3.2. *Strain and damage localization*

For most tests, axial strain is measured simultaneously by LVDT sensors, which provides a global measurement, and an axial gauge that offers a local measurement. These two measurements are complementary and allow evaluating sample strain homogeneity during testing. Figure 9 displays the curves of axial stress vs. strains measured with the gauge and the LVDT sensor for the TRX50 and TRX200 tests. It clearly indicates, for each test, the difference between global axial strain and local axial strain.

For the TRX50 test, the level of strain remains very consistent until reaching the peak stress (ε_x=3.5%); beyond this peak however, strain measured by the gauge is very low whereas the mean strain is very high. This loss of strain homogeneity at the peak stress level is visible for most tests at low confinement levels; it reveals strain localization, a characteristic of the type of concrete damage behavior. This localization phenomenon has also been observed by Rutland for tests at low confinement on a similar concrete (Rutland *et al.* 1997). On the other hand, for the TRX200 test, the strain measured by the gauge is consistent with the mean sample strain during the entire test period. This would also be true for tests at a higher

confinement level. At high confinements, the strain measured on the gauge scale remains homogeneous in the sample beyond failure.

The triaxial test results show that confinement influence on deviatoric behavior is very significant, by virtue of determining the cement matrix state before the axial compression phase. Figure 10 displays the strain limit states in the (q,σ_m) plane with their associated failure facies. These states correspond to the contraction-dilatancy transition on the triaxial volumetric curve. At low confinement ($p<p_e$), the cement matrix is only slightly damaged. Failure is caused by a mechanism of considerable localized damage at the sample scale and is to be associated with a loss in strain homogeneity; this failure is characterized by a peak stress that reveals the brittle behavior of concrete. A strong decrease in axial stiffness coupled with an increase in Poisson's ratio can be observed with an increase in axial strain. A hysteresis phenomenon appears during the unloading-reloading cycles and becomes very pronounced after the peak stress. The concrete behavior is cohesive-brittle and governed by damage phenomena, in the sense of stiffness loss.

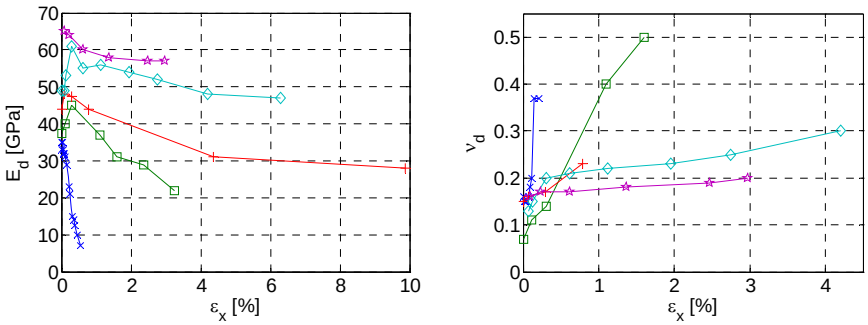

Figure 8. Evolution in elastic stiffness (left) and Poisson's ratio (right) with deviatoric axial strain at various pressures: (×) SC, (□) TRX20, (+) TRX50, (◊) TRX200, (☆) TRX400

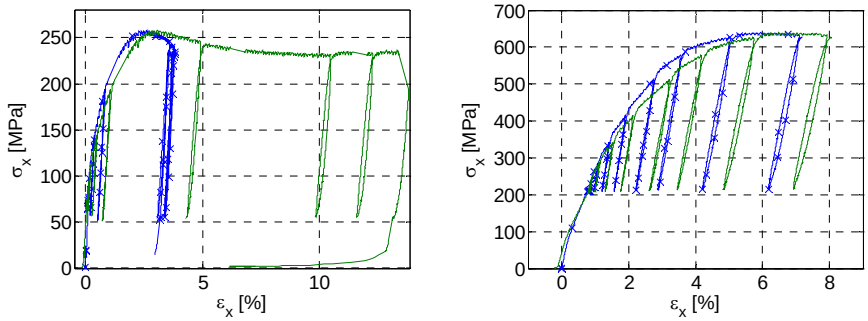

Figure 9. Comparison of axial stress-strain curves obtained by the axial gauge (×) and the LVDT sensor (-) for two triaxial tests - TRX 50 (left) and TRX 200 (right).

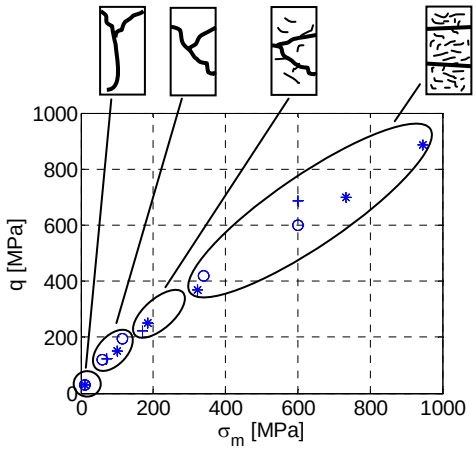

Figure 10. Limit state points as contraction-dilatancy transitions on the volumetric behavior curves plotted in the stress space (σ_m, q) with associated failure facies: (∗) Monotone triaxial tests (o) Cyclic triaxial tests (+) Proportional tests (see Gabet *et al.* 2008 for details on these tests).

Under high confinement ($p>p_c$), the cement matrix loses a significant part of its cohesion during the hydrostatic phase. Failure under an axial load is thus caused by diffuse damage without any loss of strain homogeneity. This failure is associated with a concrete behavior that becomes dilating without reaching a peak stress. The concrete is also very ductile, with both the hysteresis phenomenon and evolution in its elastic characteristics becoming negligible during unloading cycles. Concrete behavior tends toward that of granular material governed by plasticity, whereas the damage phenomenon observed at low confinement is inhibited.

4. Mesoscopic modeling

The objective of the mesoscopic modeling is first to better understand the mechanisms controlling concrete behavior under high confinement, by accessing the stress and strain states of the constitutive materials. This mesoscopic modeling also aimed at building a tool that characterizes the triaxial behavior of multiple concrete formulations without performing an extensive experimental campaign for each concrete. Indeed, uniaxial compression tests are systematically carried out whenever a concrete is used, but it is economically infeasible to carry out as many triaxial tests. For this reason, numerical modeling is intended to complement experimental tests, in predicting the triaxial behavior of various concrete formulations under high confinement (Figure 11).

Variations across concrete formulations can be divided into two basic categories: cement paste variations (water-cement ratio, porosity, fine sand, additives), and aggregate variations (volume, particle size distribution and mechanical

characteristics). A numerical concrete must be able to reproduce these variations and their consequences on global behavior. The mesoscopic model therefore contains two phases, a mortar (cement paste and fine sand) and inclusions (aggregates).

This study places emphasis on generating a good description of the behavior of the mortar used within the reference concrete (R30A7) which has undergone extensive high-confinement testing (see previous part of the paper). The mortar, labeled MR30A7, is composed of the same mixture as the R30A7 concrete, yet without the aggregate category larger than 2mm in typical size, which in fact represents 40% in volume of the R30A7 composition (Figure 12).

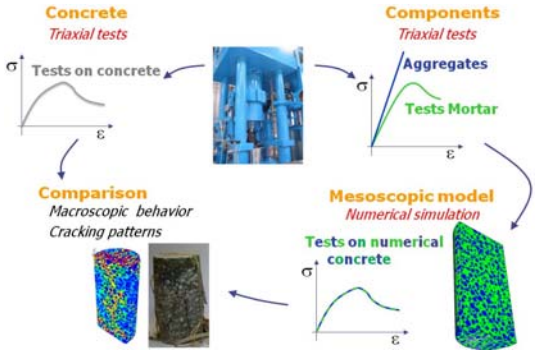

Figure 11. Principle and objectives of the mesoscopic modeling.

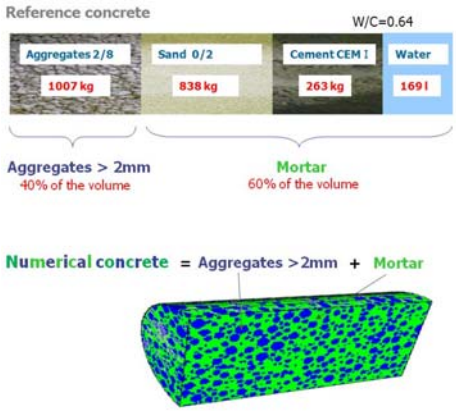

Figure 12. Scales and components of the mesoscopic modeling.

4.1. *Mortar behavior*

4.1.1. *Identification of the coupled PRM model parameters for the mortar*

The coupled PRM model is an explicit damage-plasticity model that reproduces the unilateral damage phenomena at low mean stress as well as the nonlinear compaction and plasticity phenomena at high mean stresses, phenomena that have been underlined as the most important (Burlion *et al.* 2001). In between the extremes and for high strains, the model combines these two effects. It has been described by Rouquand (Rouquand *et al.* 2007) and is based on both a damage model, i.e. the PRM model (Mazars 1986, Rouquand *et al.* 1996 and Pontiroli 1995) and the KST model for plasticity (Krieg 1972, Swenson *et al.* 1983).

4.1.2. *Identification of the coupled PRM model parameters for the mortar*

In order to perform this identification step, samples of MR30A7 were cast, and dried after hardening, then submitted to the following tests: unconfined compression, three-point-bending, hydrostatic compression and triaxial compression. Unconfined compression samples were instrumented with two axial gauges and one circumferential gauge, to allow for identification of Young's modulus and Poisson's ratio, in addition to compressive strength. The identified parameters were: E = 25.5GPa, $\nu = 0.16$ et $f_c = 59.5$MPa. The comparison between this model and the experimental test is shown in Figure 13 (left). These parameters define the entire shape of the curve and hence do not offer the possibility of adjusting the strain at peak stress to the experimentally-derived strain. Anyway, this set of parameters provides a satisfactory fit to the experimental data

Various confined tests were performed on mortar samples in order to identify parameters of the modified KST model, including volumetric behavior, in both loading and unloading (see Figure 13 right) and deviatoric behavior (not presented). These tests reveal large deformations and a much greater compaction than that observed on concrete (approximately 45% greater than those recorded on R30A7 concrete specimens in the hydrostatic phase). The initial deviatoric modulus is also greatly reduced, but the triaxial compressive strength under moderate confinement or the limit state under higher confinement exceeds by around 10% that observed on R30A7 (see Dupray *et al.* 2009 for more details on mortar behavior).

4.2. ***Numerical concrete***

4.2.1. *Numerical concrete model*

The mesoscale numerical concrete model distinguishes two phases within the concrete: mortar, which includes the cement paste and fine sand (less than 2mm in size), and aggregates. The two-dimensional approach was first seen, and is still used

in the area of thermal damage (Menou *et al.* 2008), with refined approaches (Pedersen *et al.* 2007) or shock response (Riedel *et al.* 2008). But when applied in three dimensions, this kind of numerical model can only be of very recent use, due to the heavy computational requirements associated with this approach. It has been employed in a number of cases, first for shock response (Thoma *et al.* 1999), then for uniaxial compression (Wriggers *et al.* 2006), for contact detonation (Akers *et al.* 2004), and for tension and compression (Caballero *et al.* 2006). Authors give more or less importance to the distribution of aggregates. In Akers' approach, aggregates are cubic and regularly distributed whereas the approach presented herein is similar to Riedel's one.

The model is a cylinder of the same size as the experimental sample, i.e. 7 cm in diameter and 14 cm high, what is sufficient to ensure the effect of the distribution on the macro-scale behavior is as limited as possible. The mesh is cubic and regular, which means the cylindrical shape can only be approximated. The aggregates have been modeled as assemblies of elements approximating spheres. The mesh size adopted for the tests reported in this article is 2mm, which leads to a 68,110-element model, and means that modeled aggregates may be as small as 1 element (see Figure 12). To build the numerical model, the sample is considered as 100% mortar in which aggregates are placed one by one. The numerical aggregate distribution complies with the size distribution of the actual aggregates, in a histogram of 6 classes. In each class, a random distribution of aggregate centers and diameters is assigned, and the potential superposition with previous aggregates is verified. In the absence of superposition, the elements approximating spheres undergo a change in their material properties from mortar to aggregate, until the class is full. The total aggregate fraction in the actual sample is 40%, and this high percentage is difficult to obtain from such a crude model. It implies the existence of contacts (in this case, bonds) between aggregates. Therefore this model cannot reproduce relative movements between aggregates, what will be possible with finer meshes. The choice of bonded aggregates and mortar elements is justified in the case of multi-compressive loadings that are considered here. The debounding that is observed experimentally around some aggregates after such a high confinement test is only meaningful in the unloading part of the test that is not modeled here. The maximal aggregate size is 10 mm.

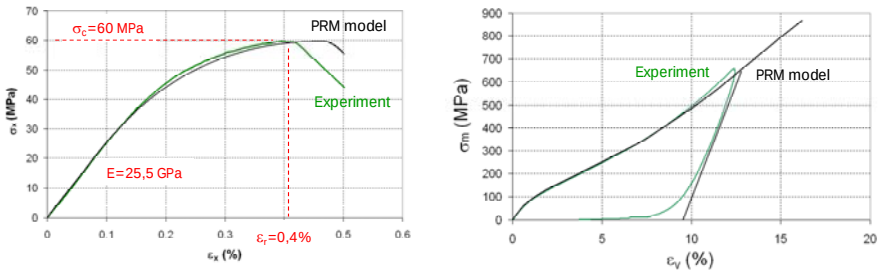

Figure 13. Identification of the coupled PRM model on the mortar behavior; unconfined compression (left) hydrostatic compression (right).

A view of the sample has been given on Figure 12. The mechanical behavior of the aggregates is selected to be elastic. The mechanical characteristics of the aggregates were not identified, but instead deduced from their chemical properties: the aggregates are mainly silicates (Si02), whose mechanical properties are available in the literature (Sellers *et al.* 1996). The Young's modulus of silicates should be set at E_{agg1}=70GPa, and Poisson's ratio at ν_{agg} = 0.2. Simple calculations, such as those performed by Riedel (Riedel *et al.* 2008), give the linear elastic parameters of the biphasic model. From this simple comparison in Young's modulus between mortar, aggregates and of actual concrete, it appears that the model would be much too steep in an uniaxial elastic compression. The main reason for this observation is the existence of the interfacial transition zone, or ITZ, that has very poor mechanical characteristics and high porosity (Scrivener *et al.* 1996). It is possible to integrate its influence in an approximate manner by simultaneously testing numerical concrete with an "aggregate" Young's modulus set at E_{agg2}=35GPa, which gives the numerical concrete the correct Young's modulus of 29GPa, and takes into account the presence of the ITZ in the "aggregate" phase of numerical concrete.

4.2.2. *Hydrostatic behavior*

The hydrostatic behavior of the numerical concrete has been assessed by means of comparison with the actual concrete. As can be seen on Figure 14, it appears that the differences between the mortar and the concrete are well replicated, with a very significant decrease in total volumetric strain, yet the numerical concrete remains too steep, even with the reduced Young's modulus of the aggregate. It should be noted that the discrepancy observed between the experimental and numerical curves is concentrated between 50 and 300MPa. The initial slopes are close, and in the range above 300MPa, the strain difference remains nearly constant at 1%. The interpretation of this phenomenon is that some physical pore collapse, happening in this range of pressures, is not reproduced in the model, and this may again be the collapse of the high-porosity ITZ. A slight difference in porosity between the mortar cast alone, non-vibrated, or cast with aggregates and vibrated, could also be a source of discrepancy.

4.2.3. *Triaxial behavior*

In order to have a global view of the capability of the numerical concrete model to describe concrete behavior under triaxial compression, the tests implemented are oriented around three aspects: axial behavior, volumetric behavior and the limit states/cracking pattern. Four levels of confinement are compared with the equivalent experimental tests: 50MPa, 200MPa, 500MPa and 650MPa (Figures 14 and 15).

Since the hydrostatic behavior of the model has already been presented, this section will focus on the deviatoric behavior. Under moderate confinement (p=50MPa) the tangent modulus of the actual concrete decreases gradually from the onset of the triaxial loading. This behavior is not reproduced by the model, wherein

damage occurs at a higher stress level and less progressively. The moduli therefore are only comparable at the beginning of the loading. The comparison between the experimental and numerical circumferential behaviors leads to better results. It is also worth noting that the numerical specimen exhibit a softening behavior. Under higher confinement (p=200MPa), we can observe more similarities between the numerical and experimental concrete. The tangent modulus of the numerical concrete is close to that of the actual concrete up until half the loading, yet the same observations as in the 50MPa case can still be made here. The initial very high slope of the experimental test is correlated with the creep occurring between the end of the hydrostatic phase and the beginning of the triaxial loading. It is clear that the numerical deviatoric behavior is not linear, which means that the numerical concrete, with the coupled PRM model, is able to reproduce damage behavior at this level: this would not be possible with the coupled PRM model when used in a monophasic sample. This phenomenon is easily explained by the presence of aggregates, which causes stress concentrations in between aggregates, in a mortar where the mean pressure remains quite low (160MPa). The results from tests conducted under very high confinement (p=650MPa) show a better correlation between numerical and experimental behavior, as the damaging behavior of the actual concrete is less obvious under high pressure since mortar damage process has already been completed by the hydrostatic pressure.

4.2.4. *Volumetric behavior and limit states*

In addition to what has already been discussed regarding the hydrostatic phase, it appears that the volumetric behavior of numerical concrete in the triaxial phase fits the experimental behavior better with increasing confining pressure (see Figure 14). For the 50MPa confinement test, the experimental volumetric behavior is considerably away from the hydrostatic curve, whereas the numerical curve lies close to this behavior. The peak-stress level is comparable but softening is more pronounced than expected. Results are much better at 200MPa, since the volumetric behavior shows greater similarity, and the stress level of the actual limit state is accurately described by the peak stress of the numerical model, as was initially intended. But again softening appears instead of the observed dilatancy. At this level, the influence of aggregate modulus on the limit state remains limited. At 650MPa, the volumetric curves of the numerical tests in the triaxial phase are very similar to the experimental curve. Moreover, the limit state is the same as the experimentally-derived limit state.

4.2.5. *Cracking patterns*

The ability of the model to predict the shape of fractured samples is evaluated in Figure 16. At 50MPa, the numerical sample exhibits two damage zones, a larger zone near one end of the sample, and a smaller zone near the other. These zones are not perpendicular to the sample axis and become clearly visible just after the peak. Though the slope observed in the actual sample is greater than that in the numerical model, the similarities are nonetheless remarkable.

At 200MPa, the model is able to replicate damage localization, as presented in Figure 16, in comparison with a photograph of the actual sample. The numerical sample exhibits two symmetrical damage zones, both perpendicular to the sample axis. This localization is visible before the peak, though the Figure 13 shows the sample precisely at peak stress. This is exactly what can be observed on the photograph of the actual sample.

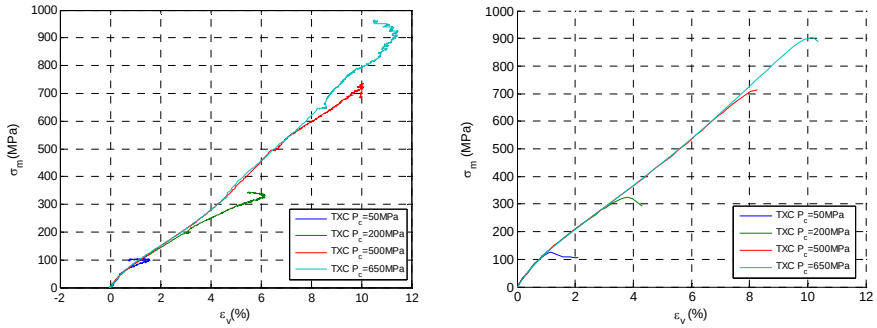

Figure 14. Triaxial tests for different confining pressure (50, 200, 500 and 650MPa): Mean stress σ_m vs. volumetric strain ε_v; experiments (left); mesoscopic modeling (right).

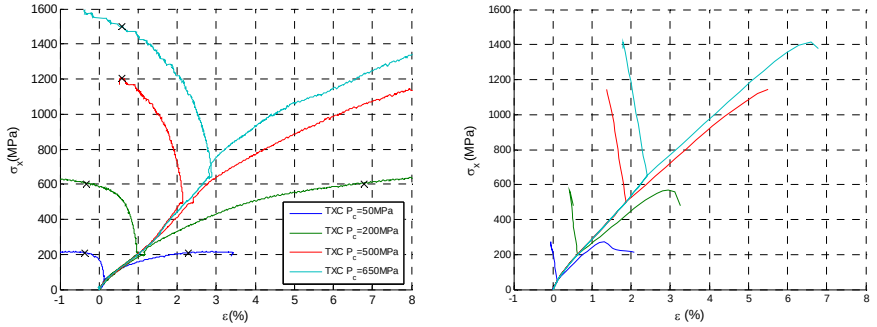

Figure 15. Triaxial tests for different confining pressure (50, 200, 500 and 650MPa): Axial stress σ_x vs. strain components ε_x and ε_θ; experiments (left); mesoscopic modeling (right).

At 650MPa, the numerical model exhibits insufficient damage in comparison with the actual sample. Damage only appears after the peak, when large plastic strains enable it. The ratio q/p rarely exceeds $3(1-2\nu)/(1+\nu)=1.75$, resulting in almost no damage. Sample axial stress is indeed affected by local plasticization, detected by a slight increase in mortar maximal compressive principal strains, the map of which is presented in Figure 16. Although not very clear in the Figure, and very affected by the presence of aggregates, the orientation of the phenomena is rather perpendicular to the axis, just as in the actual sample. When various tests are performed with slightly varying parameters or a different aggregate distribution, the observed cracking patterns are also varying but keep the same characteristics: typically the cracking bands are more or less close to the middle of the specimen, or a third horizontal band can appear at 200MPa. These variations are common on the experimental samples too.

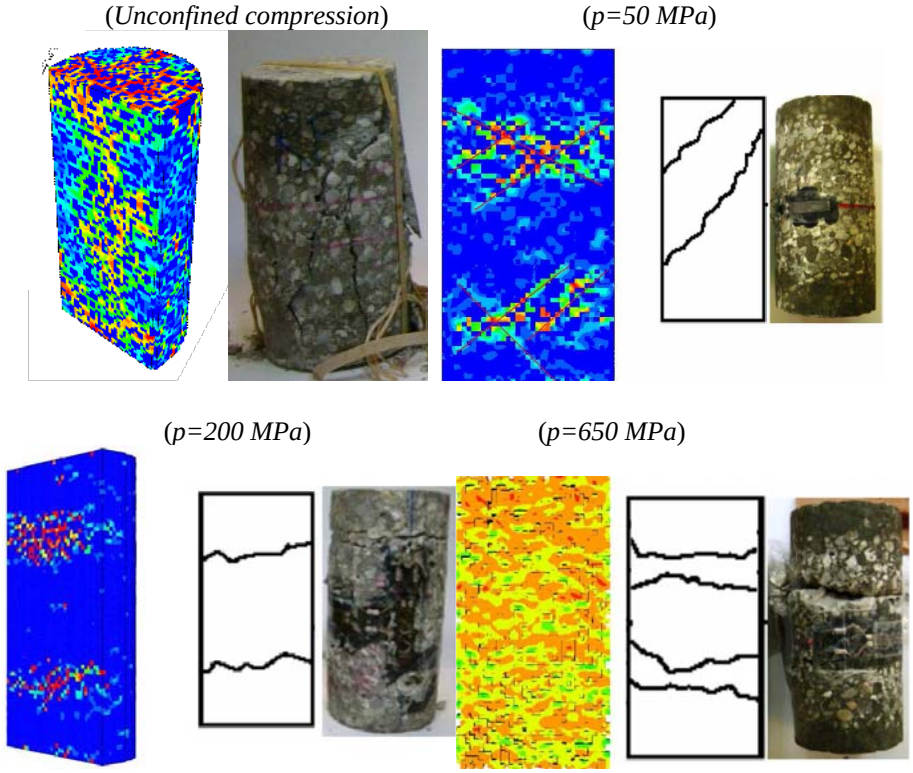

Figure 16. Damage and cracking pattern after triaxial compression tests: Comparison between experiments (right) and mesoscopic modeling (left) for different confining pressure.

5. Conclusion

This article focused on the behavior of concrete under extreme loading conditions and, in particular, has sought to characterize the evolution in triaxial behavior of a standard concrete for confining pressure varying from 0 to 650 MPa. To proceed, hydrostatic and triaxial tests containing unloading-reloading cycles have been conducted on concrete samples using a high-capacity triaxial press. These tests have allowed identifying the evolution in elastic characteristics associated with unloading concrete vs. both confinement and axial strain. Moreover, optical observations were performed in order to visualize the evolution in concrete damage pattern at the sample center.

The cyclic hydrostatic test shows that the greatest part of cement matrix damage when submitted to hydrostatic compression occurs between 60 and 150 MPa; this test has allowed determining two confining pressures that characterize concrete behavior. Under hydrostatic loading, the concrete is linear elastic for a confining pressure of less than 60 MPa. Beyond a confining pressure of 150 MPa, it is of the elastoplastic type, such as a consolidated granular material.

Although the numerical model used herein is a very simplified view of the mesoscale mechanics in concrete, it already provides a reproduction of the main characteristics of concrete behavior under high confinement, both qualitatively and quantitatively: mortar compaction, damage localization, aggregate influence on the limit state with respect to mortar, and load path influence on volumetric behavior. The fact that it correctly reproduces the damage zones observed on actual samples suggests that this model can help in the understanding of mesoscale phenomena and their influence on macroscale behavior. It clearly appears that the simple presence of aggregates induces a sizable difference with mortar behavior, not only in terms of rigidity, but throughout the hydrostatic phase, and in the second half of the deviatoric curve.

During the hydrostatic phase, the presence of aggregates causes a major decrease in mean pressure of the concrete mortar phase in comparison with the mortar alone. The consequence of this finding is that the deviatoric behavior of concrete at a given confinement does not depend on the deviatoric strength of the mortar at the same confinement, but instead at a significantly lower confinement. Further numerical tests are being performed in order to include some well-known facts about the mesoscale mechanics of concrete, including the presence of an interfacial transition zone (ITZ), and differences in mortar characteristics when cast either alone or with aggregates (greater porosity and all the ensuing consequences).

Acknowledgments

The GIGA press has been installed in the 3S-R Laboratory within the scope of a cooperative agreement signed with the French Defense Ministry's Armament Division. This research has been performed with the financial support of the Délégation Générale pour l'Armement, Centre d'Etudes de Gramat (DGA, CEG). We would like to thank Dr. Christophe Pontiroli (CEG) for giving technical and scientific advice.

8. References

Akers SA, Phillips BR., Concrete modeled as an inhomogeneous material: Numerical simulations of contact detonations charges. 18th International Symposium on Military Aspects of Blast and Shock, Bad Reichenhall, Germany, 2004.

Balmer GG Shearing strength of concrete under high triaxial stress : Computation of Mohr's Ennveloppe as a curve. Structural Research Laboratory, Report sp n°23, Denver, 1949.

Bazant ZP, Bishop FC, Chang TP. Confined compression tests of cement paste and concrete up to 300 ksi. ACI Journal 1986; 33:553-560.

Burlion N, Pijaudier-Cabot G and Dahan N, Experimental analysis of compaction of concrete and motar. Int J for Numerical and Analytical Methods in Geomechanics, 2001, 25:1467-1486

Caballero A, Carol I, Lopez CM. A meso-level approach to the 3d numerical analysis of cracking and fracture of concrete materials. Fatigue & Fracture of Engineering Materials and Structures, 2006, 29(12):979-991.

Diamond S, Huang J, The ITZ in concrete – a different view based on image analysis and SEM observations. Cement & Concrete Composites, 2001, 23:179-188

Dupray F, Malecot Y, Daudeville L, Buzaud E, A mesoscopic model for the behaviour of concrete under high confinement, International Journal for Numerical and Analytical Methods in Geomechanics, 2009, DOI: 10.1002/nag.771

Forquin P, Gary G, Gatuingt F, A testing technique for concrete under confinement at high rates of strain, Int J of Impact Engineering, 2008, 6:425-446

Gabet T., Vu X.H., Malecot Y. and Daudeville L., A new experimental technique for the analysis of concrete under high triaxial loading, Journal de Physique IV, 2006, 134, 635-644. DOI : 10.1051/jp4:2006134098

Gabet T., Malecot Y., Daudeville L., Triaxial behavior of concrete under high stresses: Influence of the loading path on compaction and limit states, Cement and Concrete Research, 2008, 38(3), 403-412.

Imran I, Pantazopoulou SJ, Experimental study of plain concrete under triaxial stress. ACI Mater J, 1996, 93(6):589-601

Jiang LH, Huang DH and Xie NX, Behavior of concrete under triaxial compressive-compressive-tensile stresses. ACI Mater J, 1991, 88(2):181-185

Krieg R. A simple constitutive description for soils and crushable foams. Technical Report SC-DR-72-0883, Sandia National Laboratories, Albuquerque 1972.

Kupfer HB, Gerstle KH, Behavior of Concrete under Biaxial Stresses. J of the Eng Mechanics Div, 1973, 99(4):853-866

Li H, Pugh D, Mechanical behavior of materials under pressure. Elsevier, Amsterdam, 1970.

Mazars J. A description of micro- and macroscale damage of concrete structures. Engineering Fracture Mechanics, 1986, 25(5-6):729-737.

Menou A, Mounajed G, Boussa H, La Borderie C, Lefdi K. Thermal damage approach of concrete: Application to specimens subjected to combined compressive and high temperature loads. High Temperature Materials and Processes, 2008; 27(1):23-39.

Pedersen RR, Simone A, Sluys LJ, Multiple-scale analysis of impact fracture. IX International Conference on Computational Plasticity, Owen DRJ, Onate E, Suarez B (eds.), Barcelona, Spain, 2007.

Poinard C., Malecot Y., Daudeville L., Damage of concrete in a very high stress state: Experimental investigation, Materials and Structures, 2009, DOI 10.1617/s11527-008-9467-6

Pontiroli C, Comportement au souffle de sturctures en béton armé, analyse expérimentale et modélisation. Thèse de doctorat, ENS Cachan, CEG 1995.

Riedel W, Wicklein M, Thoma K. Shock properties of conventional and high strength concrete: Experimental and mesomechanical analysis. International Journal of Impact Engineering, 2008, 35:155-171.

Rouquand A, Pontiroli C, Mazars J. Concrete structures under severe loading: A strategy to model the response for a large range of dynamic loads. Fracture Mechanics of Concrete and Concrete Structures: Proceedings of FraMCoS-6, Catania, Italy, 2007.

Rouquand A, An explicit damage model for dynamic concrete behavior. numerical simulations and comparisons with experimental results on reinforced concrete plates under blast loading. International conference on structures under shock and impact, Udine, Italy, 1996. DOI: 10.2495/SUSI960301.

Rutland CA, Wang ML, The effects of confinement of failure orientation in cementitious materials: Experimental observations. Cement & Concrete Composites, 1997, 19:149-160.

Schmidt MJ, Cazacu O, Green ML. Experimental and theoretical investigation of the high-pressure behavior of concrete. International Journal for Numerical and Analytical Methods in Geomechanics, 2008, DOI: 10.1002/nag.700.

Scrivener KL, Nemati KM, The percolation of pore space in the cement paste/aggregate interfacial zone of concrete. Cement and Concrete Research, 1996, 26(1):35-40.

Sellers E, Scheele F, Prediction of anisotropic damage in experiments simulating mining in Witwatersrand quartzite blocks. Int. J. Rock Mech. Min. Sci. and Geomech. Abstr. 1996, 33(7):659-670.

Sfer D, Ignacio C, Gettu R, Etse G, Study of behavior of concrete under triaxial compression. Journal of Engineering Mechanics, 2002, 128(2):156-163

Swenson DV, Taylor LM, A finite element model for the analysis of tailored pulse simulation of boreholes. International Journal for Numerical and Analytical Methods in Geomechanics, 1983, 7(4):469-484.

Taliercio A, Berra M, Pandolfi A, Effect of high-intensity sustained triaxial stresses on the mechanical properties of plain concrete. Mag Concrete Res, 1999, 51(6):437-447

Thoma K, Riedel W, Hiermaier S. Mesomechanical modeling of concrete shock response experiments and linking to macromechanics by numerical analysis. Proceedings of European Conference on Computational Mechanics, Munchen, Germany, 1999.

Torrenti JM, Benajia EH, Boulay C, Influence of boundary conditions on strain softening in concrete compression test. ASCE J of Engreg Mech, 1993, vol. 119 n°12.

Vu X.H., Malecot Y., Daudeville L, Strain measurements on porous concrete samples for triaxial compression and extension tests under very high confinement, Journal of strain analysis for engineering design, 2009, in press.

Vu X.H., Malecot Y., Daudeville L., Buzaud E., Experimental analysis of concrete behavior under high confinement: Effect of the saturation ratio, International Journal of Solids and Structures, 2009, 46, 1105-1120. doi:10.1016/j.ijsolstr.2008.10.015

Vu X.H., Malecot Y., Daudeville L., Buzaud E., Effect of the water/cement ratio on concrete behavior under extreme loading, International Journal for Numerical and Analytical Methods in Geomechanics, 2009, DOI: 10.1002/nag.796.

Wang CZ, Guo ZH and Zhang XQ, Experimental investigation of biaxial and triaxial compressive concrete strength. ACI Mater J, 1987, 84:92-100

Warren T, Fossum A, and Frew D, Experimental investigation of size effect in concrete fracture under multiaxial compression into low-strength (23 MPa) concrete: target characterization and simulations. Int J of Impact Engineering, 2004, 30:477-503

William EM, Akers SE and Reed PA, Constitutive models for the triaxial behavior of concrete. Report ERDC/GSL TR-05-16 Geotechnical and Structures Laboratory, US Army, 2005.

Wriggers P, Moftah SO, Mesoscale models for concrete: Homogenisation and damage behavior. Finite Elements in Analysis and Design, 2006, 42(7):623-636.

Zukas JA, Penetration and perforation of solids, Impact Dynamics. Krieger Publishing Company, 1992.